

Ternary fission within the temperature dependent relativistic mean field approach

M.T. Senthil kannan^{1,*}, Bharat Kumar^{2,4}, M. Balasubramaniam¹, B. K. Agrawal^{3,4}, and S. K. Patra^{2,4,†}

¹*Department of Physics, Bharathiar University, Coimbatore - 641046, India.*

²*Institute of Physics, Sachivalaya Marg, Bhubaneswar - 751005, India.*

³*Saha Institute of Nuclear Physics, 1/AF, Bidhannagar, Kolkata - 700064, India. and*

⁴*Homi Bhabha National Institute, Anushakti Nagar, Mumbai - 400094, India.*

(Dated: November 13, 2018)

For the first time, we apply the temperature dependent relativistic mean field (TRMF) model to study the ternary fission of heavy nucleus using level density approach. The probability of yields of a particular fragment is obtained by evaluating the convolution integrals which employ the excitation energy and the level density parameter for a given temperature calculated within the TRMF formalism. To illustrate, we have considered the ternary fissions in ^{252}Cf , ^{242}Pu and ^{236}U with fixed third fragment $A_3 = ^{48}\text{Ca}$, ^{20}O and ^{16}O respectively. The relative yields are studied for the temperatures $T = 1, 2$ and 3 MeV. For the comparison, the relative yields are also calculated from the single particle energies of the finite range droplet model (FRDM). In general, the larger phase space for the ternary fragmentation is observed indicating that such fragmentations are most probable ones. For $T = 2$ and 3 MeV, the Sn + Ni + Ca is the most probable combination for the nucleus ^{252}Cf . However, for the nuclei ^{242}Pu and ^{236}U , the maximum fragmentation yields at $T = 2$ MeV differ from those at $T = 3$ MeV. For $T = 3$ MeV, the closed shell ($Z = 8$) light mass fragments with its corresponding partners has larger yield values. But, at $T = 2$ MeV Si/P/S are favorable fragments with the corresponding partners. It is noticed that the symmetric binary fragmentation along with the fixed third fragment for ^{242}Pu and ^{236}U are also favored at $T = 1$ MeV. The temperature dependence of the nuclear shape and the single particle energies are also discussed.

PACS numbers: 25.85.-w, 21.10.Ma, 21.10.Pc, 24.75.+i

I. INTRODUCTION

The exotic decay modes other than basic decay modes of heavy nuclei are needed to be studied to understand the reaction kinematics and the structure as well. One such exotic fission mode of heavy nuclei is the splitting into three charged fragments so-called ternary fission. After the earlier reports on ternary fission [1, 2], the extensive experimental studies on the heavy nuclei ^{252}Cf , ^{242}Pu and ^{236}U were reported [3–6]. The observations indicate that alpha particle have the larger yield values. Köster *et al.* [5] reported the ternary fission yields of ^{242}Pu for the various third fragment isotopes up-to ^{30}Mg . Pyatkov *et al.* [6, 7] reported the ternary fission yields of ^{252}Cf (sf) and ^{236}U (n_{th} , f) using the missing mass approach. The Sn+Ni/Ge+Ca/S are the most favorable combinations. But theoretically, Fong [8] calculated the probability of α particle accompanied fission using statistical theory. Diehl *et al.* [9] applied the liquid drop model to study of the true ternary fission (TTF) where the three fragments are almost equal by direct prolate/oblate and cascade ternary fission modes. The authors reported that prolate mode is energetically more favorable than the oblate fission mode. Rubchenya *et al.* [10] applied the dynamical model for the ternary fission and reported the formation of light charged particle (LCP) at later descent stage from the saddle to scission point. Oertzen and Nasirov [11] obtained the TTF fragments using the potential energy surface (PES) calculations. Manimaran *et al.* [12] proposed the three cluster model (TCM) to study the α parti-

cle ternary fission. The obtained relative yield are very well in agreement with the experimental data. Further, TCM is applied to the study of equatorial and collinear configuration [13] of all possible third fragments. The collinear configuration is more favorable for the heavy third particle accompanied fission with the third fragment at the middle of two fragments. Rajasekaran and Devanathan [14] applied the statistical theory to study the binary mass distributions using the single particle energies of the Nilsson model. The obtained results were well in agreement with the experimental data. As the sequel of this work, Balasubramaniam *et al.* [15] studied the ternary mass distribution of ^{252}Cf for the fixed third fragment ^{48}Ca using the single particle energies of the finite range droplet model (FRDM) and obtained the Sn + Ni + Ca as the most favorable combination at $T = 2$ MeV. Further, the authors extended [16] the study to calculate the ternary charge distribution of potential energy minimized possible fragments whose probability were calculated using the convolution integrals. The results indicate that Sn is the one of the most favorable combination for temperature $T = 2$ MeV. The excitation energies and the level density parameters for different fission fragments required to evaluate the convolution integrals in such calculations were obtained using temperature independent single-particle energies from the FRDM corresponding to the ground state deformations. The temperature dependence was incorporated through the Fermi-Dirac distributions.

The single-particle energies are usually sensitive to the temperature in heavy nuclei, in particular, due to the transition from the deformed to the spherical shape and the transition from pairing phase to the normal phase as induced by temperature. Such features can significantly affect the temperature dependence of the excitation energy and the level density

*Electronic address: senthilthulasiram@gmail.com

†Electronic address: patra@iopb.res.in

parameter. The temperature induced effects on the nuclear deformation and the pairing phase can be readily accounted for within the temperature dependent non-relativistic and relativistic mean-field models in self-consistent manner. Of the main focus in the present investigation is the relativistic mean-field models (RMF). The RMF models at zero temperature [17–21] with various parameter sets have successfully reproduced the bulk properties, such as binding energies, root mean square radii, quadrupole deformation etc. not only for nuclei near the β stability line but also for nuclei away from it. The temperature dependent relativistic mean field (TRMF) model has been employed to study the structural properties of the highly excited hot nuclei [22]. The heavy and rare earth nuclei are studied within the TRMF model [23, 24] which indicate that there is a phase transition from the pairing phase to normal phase around the temperature $T \sim 0.8$ MeV and shape transition from prolate to spherical shape at critical temperature $T_c \sim 2.7$ MeV.

The RMF formalism is successfully applied to the study of clusterization of the known cluster emitting heavy nuclei [25–27]. The presence of α -clusters in light nuclei, such as ^{12}C , which is also an experimental fact is explained very convincingly within the framework of RMF approximation. In addition, it is claimed that the $N \neq Z$ clusters exit in the excited states of heavy nuclei. For superheavy nuclei, the existence of $N \approx Z$ matter is predicted by this theory. The ternary cluster decay from the hyper-hyper deformed ^{56}Ni at high angular momenta which is formed in the $^{32}\text{S} + ^{24}\text{Mg}$ reaction is reported in Ref. [28]. The RMF model predicted the two multiple $N = Z$, α like clusters or symmetric fission mode of hyper-hyper deformed ^{56}Ni nucleus [29] which is in contradiction with the experimental results. However, the multiple α -nucleus clusterization is in agreement with earlier experiments. Rutz *et al.* [30] reproduced the double, triple humped fission barrier of ^{240}Pu , ^{232}Th and the asymmetric ground states of ^{226}Ra using RMF formalism. Moreover, the symmetric and asymmetric fission modes are also successfully reproduced. Patra *et al.* [31] studied the neck configuration in the fission decay of neutron rich U and Th isotopes. Further, various decay modes, such as α -decay, β -decay and cluster decays are studied in Refs. [32–36] using RMF formalism with double folding M3Y, LR3Y and NLR3Y nucleon-nucleon interaction potential within the preformed cluster model.

In the present work we studied the ternary fission of heavy

nuclei ^{252}Cf , ^{242}Pu and ^{236}U using the temperature dependent relativistic mean field (TRMF) model. The various inputs, like, single particle energies, excitation energies and the level density parameters of the fission fragments are calculated using the TRMF model with the well known NL3 parameter set [37]. For comparison, we calculate the ternary mass distributions using the single particle energies of FRDM as explained in Ref. [16].

The article is organized as follows. Section II provides a brief description of statistical theory and the TRMF with inclusion of BCS pairing formalism used for this study. In section III we present our total energy calculations and the temperature dependence of the excitation energies, β_2 , single particle energies. Further, we discuss about the ternary mass distribution of heavy nuclei and the temperature dependence of level density parameter and the level density. The main results are summarized in Sec. IV.

II. FORMALISM

We generate different combinations of ternary fission fragments by considering their charge to mass ratio to be equal to that of the parent nucleus [14, 15] i.e.,

$$\frac{Z_P}{A_P} \approx \frac{Z_i}{A_i} \quad (1)$$

where A_P , Z_P and A_i , Z_i ($i = 1, 2$, and 3) correspond to mass and charge number of the parent nucleus and three fission fragments, respectively. The following constraints, $A_1 + A_2 + A_3 = A$, $Z_1 + Z_2 + Z_3 = Z$, and $A_1 \geq A_2 \geq A_3$ are imposed to satisfy the conservation of mass and charge number in nuclear reaction and to avoid the repetition of fragment combinations. The third fragment A_3 is also considered a priori to find the other two fragments A_1 and A_2 .

A. Statistical Theory

According to the statistical theory [14, 16, 38, 39], the ternary fission probability $P(A_j, Z_j)$ is proportional to the folded densities $\rho_{123}(A_i, Z_i, E^*)$ of the three distinct fragments and is given by,

$$\rho_{123}(A_i, Z_i, E^*) = \int_0^{E^*} \rho_1(A_1, Z_1, E_1^*) \left[\int_0^{E^*} \int_0^{E^*} \prod_{i=2}^3 \rho_i(A_i, Z_i, E_i^*) \delta(E_2^* + E_3^* - (E^* - E_1^*)) dE_i^* \right] dE_1^*, \quad (2)$$

with E^* as the excitation energy. Here, ρ_i is the level density of three fragments ($i = 1, 2, 3$). The double integral in the square bracket is the binary convolution integral. The nuclear level density [39, 40] is expressed as a function of fragment excitation energy E_i^* and the single particle level density pa-

rameter a_i is,

$$\rho_i(E_i^*) = \frac{1}{12} \left(\frac{\pi^2}{a_i} \right)^{1/4} E_i^{*(-5/4)} \exp \left(2\sqrt{a_i E_i^*} \right). \quad (3)$$

In the Refs. [15, 16], we calculated the excitation energies of the fragments using the single particle energies of FRDM [41] at a given temperature T . In the present work we applied the self consistent temperature dependent relativistic mean field theory to calculate the excitation energy of the fragments. The excitation energy is calculated as,

$$E_i^*(T) = E(T) - E(T = 0). \quad (4)$$

The level density parameter a_i is given as,

$$a_i = \frac{E_i^*}{T^2}. \quad (5)$$

The relative yield is calculated as the ratio between the probability of a given ternary fragmentation and the sum of the probabilities of all the possible ternary fragmentations and it is given by,

$$Y(A_j, Z_j) = \frac{P(A_j, Z_j)}{\sum_j P(A_j, Z_j)}. \quad (6)$$

The competing basic decay modes such as neutron emission, α decay, binary fragmentation are not considered in the present work. The presented results are the prompt disintegration of a parent nucleus into three fragments (democratic breakup). The resulting excitation energy would be liberated as prompt particle emission or delayed emission, but such secondary emissions are not considered in the present study.

B. RMF Formalism

The RMF theories assume that the nucleons interact with each other via the meson fields. The nucleon - meson interaction is given by the Lagrangian density [17–19, 21, 42, 43],

$$\begin{aligned} \mathcal{L} = & \bar{\psi}_i \{ i\gamma^\mu \partial_\mu - M \} \psi_i + \frac{1}{2} \partial^\mu \sigma \partial_\mu \sigma - \frac{1}{2} m_\sigma^2 \sigma^2 \\ & - \frac{1}{3} g_2 \sigma^3 - \frac{1}{4} g_3 \sigma^4 - g_\sigma \bar{\psi}_i \psi_i \sigma \\ & - \frac{1}{4} \Omega^{\mu\nu} \Omega_{\mu\nu} + \frac{1}{2} m_\omega^2 V^\mu V_\mu - g_\omega \bar{\psi}_i \gamma^\mu \psi_i V_\mu \\ & - \frac{1}{4} \vec{B}^{\mu\nu} \cdot \vec{B}_{\mu\nu} + \frac{1}{2} m_\rho^2 \vec{R}^\mu \cdot \vec{R}_\mu - g_\rho \bar{\psi}_i \gamma^\mu \vec{\tau} \psi_i \cdot \vec{R}^\mu \\ & - \frac{1}{4} F^{\mu\nu} F_{\mu\nu} - e \bar{\psi}_i \gamma^\mu \frac{(1 - \tau_{3i})}{2} \psi_i A_\mu. \end{aligned} \quad (7)$$

Where, ψ_i is the single particle Dirac spinor. The arrows over the letters in the above equation represent the isovector quantities. The nucleon, the σ , ω , and ρ meson masses are denoted by M , m_σ , m_ω and m_ρ respectively. The meson and the photon fields are denoted by σ , V_μ , R^μ and A_μ for σ , ω , ρ -mesons and photon respectively. The g_σ , g_ω , g_ρ and $\frac{e^2}{4\pi}$ are the coupling constants for the σ , ω , ρ - mesons and photon fields with nucleons respectively. The strength of the constants g_2 and g_3 is responsible for the nonlinear coupling of σ meson

(σ^3 and σ^4). The field tensors of the isovector mesons and the photon are given by,

$$\Omega^{\mu\nu} = \partial^\mu V^\nu - \partial^\nu V^\mu, \quad (8)$$

$$\vec{B}^{\mu\nu} = \partial^\mu \vec{R}^\nu - \partial^\nu \vec{R}^\mu - g_\rho (\vec{R}^\mu \times \vec{R}^\nu), \quad (9)$$

$$F^{\mu\nu} = \partial^\mu A^\nu - \partial^\nu A^\mu. \quad (10)$$

The classical variational principle gives the Euler-Lagrange equation, we get the Dirac-equation with potential terms for the nucleons and Klein-Gordan equations with source terms for the mesons. We applied the no-sea approximation, so we neglected the antiparticle states. We are dealing with the static nucleus, so the time reversal symmetry and the conservation of parity simplifies the equations. After simplifications, the Dirac equation for the nucleon is given by,

$$\{-i\alpha \cdot \nabla + V(r) + \beta [M + S(r)]\} \psi_i = \epsilon_i \psi_i, \quad (11)$$

where $V(r)$ represents the vector potential and $S(r)$ is the scalar potential,

$$\begin{aligned} V(r) &= g_\omega \omega_0 + g_\rho \tau_3 \rho_0(r) + e \frac{(1 - \tau_3)}{2} A_0(r) \\ S(r) &= g_\sigma \sigma(r), \end{aligned} \quad (12)$$

which contributes to the effective mass,

$$M^*(r) = M + S(r). \quad (13)$$

The Klein-Gordon equations for the meson and the electromagnetic fields with the nucleon densities as sources are,

$$\{-\Delta + m_\sigma^2\} \sigma(r) = -g_\sigma \rho_s(r) - g_2 \sigma^2(r) - g_3 \sigma^3(r), \quad (14)$$

$$\{-\Delta + m_\omega^2\} \omega_0(r) = g_\omega \rho_v(r), \quad (15)$$

$$\{-\Delta + m_\rho^2\} \rho_0(r) = g_\rho \rho_3(r), \quad (16)$$

$$-\Delta A_0(r) = e \rho_c(3). \quad (17)$$

The corresponding densities such as scalar, baryon (vector), isovector and proton (charge) are given as

$$\rho_s(r) = \sum_i n_i \psi_i^\dagger(r) \psi_i(r), \quad (18)$$

$$\rho_v(r) = \sum_i n_i \psi_i^\dagger(r) \gamma_0 \psi_i(r), \quad (19)$$

$$\rho_3(r) = \sum_i n_i \psi_i^\dagger(r) \tau_3 \psi_i(r), \quad (20)$$

$$\rho_p(r) = \sum_i n_i \psi_i^\dagger(r) \left(\frac{1 - \tau_3}{2} \right) \psi_i(r). \quad (21)$$

To solve the Dirac and Klein-Gordan equations, we expand the Boson fields and the Dirac spinor in an axially deformed

symmetric harmonic oscillator basis with β_0 as the initial deformation parameter. The nucleon equation along with different meson equations form a set of coupled equations, which can be solved by iterative method. The center of mass correction is calculated with the non-relativistic approximation $E_{c.m.} = -3/4 \times 41A^{-1/3}$. The quadrupole deformation parameter β_2 is calculated from the resulting quadrupole moments of the proton and neutron. The total energy is given by [20, 44, 45],

$$E(T) = \sum_i \epsilon_i n_i + E_\sigma + E_{\sigma NL} + E_\omega + E_\rho + E_C + E_{pair} + E_{c.m.} - AM, \quad (22)$$

with

$$E_\sigma = -\frac{1}{2}g_\sigma \int d^3r \rho_s(r) \sigma(r), \quad (23)$$

$$E_{\sigma NL} = -\frac{1}{2}g_\sigma \int d^3r \left\{ \frac{1}{3}g_2 \sigma^3(r) + \frac{1}{2}g_3 \sigma^4(r) \right\}, \quad (24)$$

$$E_\omega = -\frac{1}{2}g_\omega \int d^3r \rho_v(r) \omega^0(r), \quad (25)$$

$$E_\rho = -\frac{1}{2}g_\rho \int d^3r \rho_3(r) \rho^0(r), \quad (26)$$

$$E_C = -\frac{e^2}{8\pi} \int d^3r \rho_c(r) A^0(r), \quad (27)$$

$$E_{pair} = -\Delta \sum_{i>0} u_i v_i = -\frac{\Delta^2}{G}, \quad (28)$$

$$E_{c.m.} = -\frac{3}{4} \times 41A^{-1/3}. \quad (29)$$

Here, ϵ_i is the single particle energy, n_i is the occupation probability and E_{pair} is the pairing energy obtained from the simple BCS formalism.

C. Pairing and temperature dependent RMF formalism

Pairing correlation plays a pivotal role in the description of the open shell nuclei and the quantitative description of deformation in heavy nuclei. In the Hartree approximation, we have only, $\psi^\dagger \psi$ (density) term in the Lagrangian. The inclusion of pairing term like $\psi^\dagger \psi^\dagger$, $\psi \psi$ and two body interaction term $\psi^\dagger \psi^\dagger \psi \psi$ violates the particle number conservation. So, we applied externally the BCS constant pairing gap approximation for our calculation to take the pairing correlation into account. The pairing interaction energy in terms of occupation probabilities v_i^2 and $u_i^2 = 1 - v_i^2$ is written as [46, 47]:

$$E_{pair} = -G \left[\sum_{i>0} u_i v_i \right]^2, \quad (30)$$

with G is the pairing force constant. The variational approach with respect to the occupation number v_i^2 gives the BCS equation [47]:

$$2\epsilon_i u_i v_i - \Delta(u_i^2 - v_i^2) = 0, \quad (31)$$

with the pairing gap $\Delta = G \sum_{i>0} u_i v_i$. The pairing gap (Δ) of proton and neutron is taken from the empirical formula [20, 48]:

$$\Delta = 12 \times A^{-1/2}. \quad (32)$$

The temperature introduced in the partial occupancies in the BCS approximation is given by,

$$n_i = v_i^2 = \frac{1}{2} \left[1 - \frac{\epsilon_i - \lambda}{\tilde{\epsilon}_i} [1 - 2f(\tilde{\epsilon}_i, T)] \right], \quad (33)$$

with

$$f(\tilde{\epsilon}_i, T) = \frac{1}{(1 + \exp[\tilde{\epsilon}_i/T])} \quad \text{and} \quad \tilde{\epsilon}_i = \sqrt{(\epsilon_i - \lambda)^2 + \Delta^2}. \quad (34)$$

The function $f(\tilde{\epsilon}_i, T)$ represents the Fermi Dirac distribution function for quasi particle energies $\tilde{\epsilon}_i$. The chemical potential $\lambda_p(\lambda_n)$ for protons (neutrons) is obtained from the constraints of particle number equations

$$\sum_i n_i^Z = Z, \quad \sum_i n_i^N = N. \quad (35)$$

The sum is taken over all proton and neutron states. The entropy is obtained by,

$$S = -\sum_i [n_i \ln n_i + (1 - n_i) \ln(1 - n_i)]. \quad (36)$$

The temperature dependent RMF total energies and the gap parameter are obtained by minimizing the free energy,

$$F = E - TS. \quad (37)$$

In constant pairing gap calculations, for a particular value of pairing gap Δ and force constant G , the pairing energy E_{pair} diverges, if it is extended to an infinite configuration space. In fact, in all realistic calculations with finite range forces, Δ is not constant, but decreases with large angular momenta states above the Fermi surface. Therefore, a pairing window in all the equations are extended up-to the level $|\epsilon_i - \lambda| \leq 2(41A^{-1/3})$ as a function of the single particle energy. The factor 2 has been determined so as to reproduce the pairing correlation energy for neutrons in ^{118}Sn using Gogny force [20, 46, 49].

III. RESULTS AND DISCUSSIONS

In earlier studies [15, 16], the level densities of the fragments were calculated using the single particle energies from the Finite Range Droplet Model (FRDM) of Möller *et. al.* [50]. The single particle levels were retrieved from the Reference Input Parameter Library (RIPL-3) [51]. In the present study, we calculate the level densities using the TRMF formalism. Before embarking on our main results, we discuss about the temperature induced structural changes in the ^{252}Cf , ^{242}Pu and ^{236}U nuclei. Next, we calculate relative yields for the ternary fission of ^{252}Cf , ^{242}Pu and ^{236}U with the fixed third fragments $A_3 = ^{48}\text{Ca}$, ^{20}O and ^{16}O respectively. The other two fragments with masses and charges A_1, Z_1 and A_2, Z_2 are obtained by keeping the mass to charge ratio to be equal to that of parent nucleus as given by Eq. (1). The results are presented for the three different temperatures $T = 1, 2$ and 3 MeV. In principle, one should consider all the possible third fragment. However, in the present study we have neglected such possibilities. From the cluster decay study of ^{252}Cf [52], it is shown that ^{48}Ca or the neighboring ^{48}Ar or ^{52}Ca have large preformation probability compared to their light clusters, such as C, O etc. In the view of experimental data [5] ^{20}O is chosen for ^{242}Pu as the third fragment.

The TRMF equations for the nucleon and the Boson fields are solved within the basis expansion method. In the present work, the number of oscillator shells $N_F = 12$ and $N_B = 20$ are used as the basis space for the nucleons and boson fields, respectively. The total energy is obtained by minimizing the free energy at a given temperature. The ground state ($T = 0$) binding energies are well reproduced with the experimental data in our calculations.

A. Excitation energies, quadrupole deformation parameter and single particle energies

The shape transitions in ^{166}Er and ^{170}Er using the TRMF formalism is studied in [23]. The shape transition occurs at $T = 2.7$ MeV. Similar studies have been performed by applying the finite temperature Hartree Fock Bogoliubov method to the finite range density dependent Gogny force [53] and the pairing plus quadrupole force [54]. These results are similar to those obtained within the TRMF formalism. At finite temperatures, the continuum corrections due to the excitation of nucleons in the continuum are to be considered. The level density in the continuum depends on the basis space parameter N_F and N_B [55]. It has been shown that the continuum corrections are not very important in the calculations of level densities up-to the temperature $T \sim 3$ MeV [23, 56]. In our present study, we neglected the continuum corrections because the considered temperatures are up to $T = 3$ MeV. Further, we do not include the thermal fluctuations due to computational limitations. The thermal fluctuations are to be included for the more quantitative study of shape transitions.

The temperature dependence of the excitation energies of the parent nuclei ^{252}Cf , ^{242}Pu and ^{236}U are shown in Fig. 1 for $T = 0-4$ MeV. The excitation energy of the nuclei in-

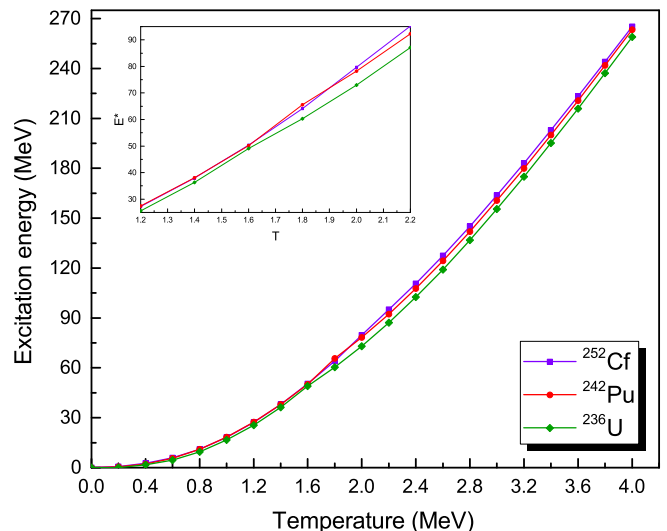


FIG. 1: (Color online) Temperature dependence of the excitation energies for the nuclei ^{252}Cf , ^{242}Pu and ^{236}U .

creases quadratically with the temperature, as given by Fermi gas approximation $E^* = aT^2$. Further, small deviations from the quadratic behavior are observed for the nuclei ^{242}Pu and ^{236}U curves (depicted inside the Fig. 1) at the temperatures $T = 1.8$ and 1.6 MeV respectively. This is due to the shape transition of the nuclei at these temperatures which is called critical temperature T_c . But, there is no such deviations seen in the case of ^{252}Cf . To clarify this we have plotted the quadrupole deformation parameter (β_2) as a function of temperature in Fig. 2. The shape transitions from prolate to spherical shape occur sharply in ^{242}Pu and ^{236}U at the critical temperatures $T_c = 1.8$ and 1.6 MeV respectively. In ^{252}Cf nucleus the deformation decreases gradually with temperature and it vanishes at $T_c = 2.2$ MeV. For the nuclei ^{242}Pu and

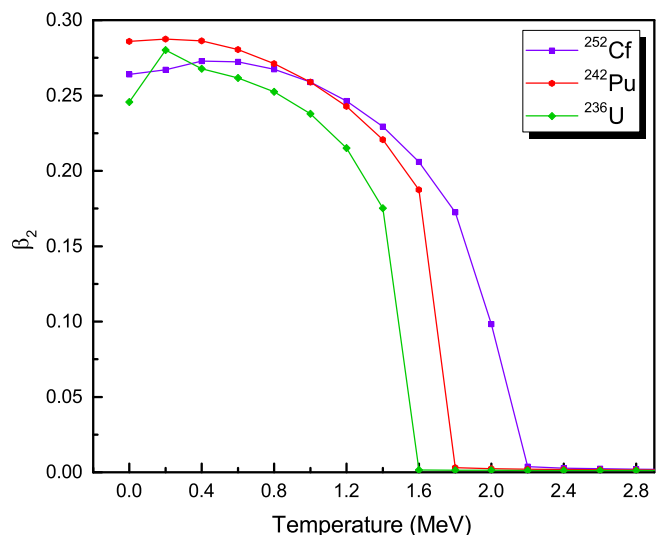


FIG. 2: (Color online) Temperature dependence of the quadrupole deformation parameter β_2 for the nuclei ^{252}Cf , ^{242}Pu and ^{236}U .

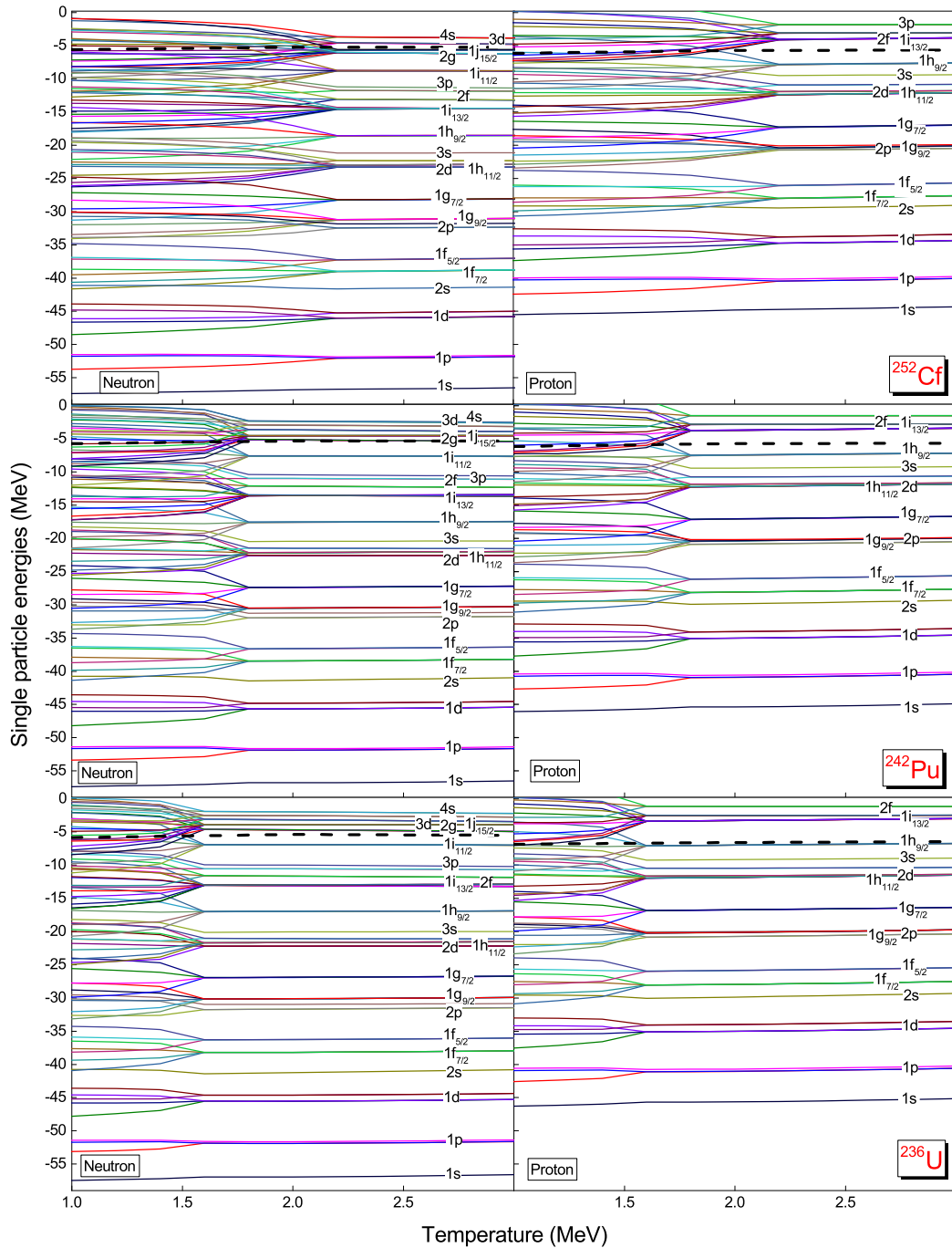


FIG. 3: (Color online) Variation of single particle levels of ^{252}Cf , ^{242}Pu and ^{236}U with temperature T . Fermi levels are denoted by the dashed line (black).

^{236}U , the β_2 increases up to $T = 0.2$ MeV due to the transitions from the pairing to normal phase. The pairing transitions occurs at $T = 0.4$ MeV for the nucleus ^{252}Cf . In earlier studies [23], the deformation parameter β_2 dropped rapidly around the transition temperature and it leveled off within the interval of $T \simeq 0.2 - 0.3$ MeV around the transition temperature.

In Fig. 3 we plot the thermal evolution of the single particle energies (spe) for the protons and neutrons for the considered nuclei. The black dashed lines in all panels repre-

sent the Fermi surface. It can be seen that various Nilsson single-particle energies become degenerate beyond T_c . When temperature increases, more levels above the Fermi surface are occupied. As a result the occupancies of non degenerate states evolves in a self consistent manner which drives the single particle potential towards spherically symmetric one. In other words, the shell structures vanishes at high temperatures and the nucleus becomes a perfect liquid drop with degenerate Fermions.

B. Ternary fission mass distribution and the level densities

Pyatkov and Oertzen group [6, 7, 57, 58] experimentally observed the heavy third fragments from the new decay mode called collinear cluster tripartition (CCT), in which the ternary fragments are collinearly emitted due to the lower Coulomb interaction for this configuration and at least one of the fragment has the composition with magic number of nucleon. Further, Pyatkov *et. al.* [6] reported that the CCT decay of ^{252}Cf with the ternary ^{48}Ca yields of $4.7 \pm 0.2 \times 10^{-3}$ / binary fission and the CCT decay of ^{236}U with the ternary ^{34}Si yields of $5.1 \pm 0.4 \times 10^{-3}$ / binary fission. It was further reported that, this yield is due to the whole *Ni-bump* consisting of some hundreds of different mass partitions. In Ref. [7], it is mentioned that the total yield of $^{68,72}\text{Ni}$ ions do not exceed 10^{-4} / binary fission. However, the yield of each separate ternary partition, for instance $^{128}\text{Sn} + ^{72}\text{Ni} + ^{52}\text{Ca}$ can be estimated to be of the order of 3×10^{-6} / binary fission. It is reported that the heavy third particle cluster like ^{48}Ca , ^{50}Ca has larger yield values in collinear configuration than the light third fragment ^4He , ^{10}Be [59]. Recently [15] studied ternary fission mass distribution of ^{252}Cf using FRDM, for the fixed third fragment ^{48}Ca , at the temperatures $T = 1$ and 2 MeV, revealed that Sn + Ni + Ca as the most favorable combination at $T = 2$ MeV. For our investigation, we consider one of the nucleus to be ^{252}Cf for the study of ternary fission at the temperatures $T = 1, 2$ and 3 MeV. The ternary mass distribution of ^{242}Pu is studied using the third fragment as ^{20}O as suggested by Köster [5]. We also studied the ternary fission of ^{236}U for the fixed cluster like third fragment ^{16}O . For the comparison, the ternary mass distributions are also calculated using the FRDM formalism.

The total energy at finite temperature and ground state energy are calculated using the TRMF formalism as discussed in the section II A. From the TRMF the excitation energy E^* of fragments are calculated using Eq. (4). From the excitation energy E^* and the temperature T the level density parameter a is calculated using Eq. (5). From the excitation energy E^* and the level density parameter a , the level density ρ of fragments are calculated using Eq. (3). From the fragment level densities ρ_i , the folding density ρ_{123} is calculated using the convolution integral Eq. (2) and the relative yield values are calculated using Eq. (6). It is to be noted that, the total yield values are normalized to 2 throughout the calculations. In FRDM formalism, the temperature dependence introduced in the Fermi occupation number. Using the Lagrange multipliers $\alpha^{N,Z}$ and β and the number equations, the temperature dependent energy $E(T)$ is calculated from the ground state single particle energies for a given temperature T . The excitation energy E^* at the given temperature is $E^* = E(T) - E(0)$ and other details can be found in Ref. [15].

In Fig. 4, the TRMF results for the ternary fission mass distributions of ^{252}Cf for the fixed third fragment ^{48}Ca are shown for different temperatures. For, $T = 1$ MeV, $^{108}\text{Nb} + ^{96}\text{Rb} + ^{48}\text{Ca}$ is the most probable fragmentation followed by emission of $^{141}\text{Xe} + ^{63}\text{Cr} + ^{48}\text{Ca}$. For higher temperatures $T = 2$ and 3 MeV, it is interesting to see that $^{132}\text{Sn} + ^{72}\text{Ni} + ^{48}\text{Ca}$ is the most favorable combination of the existing fragmentations. In Figs. 5 and 6, we display the TRMF results

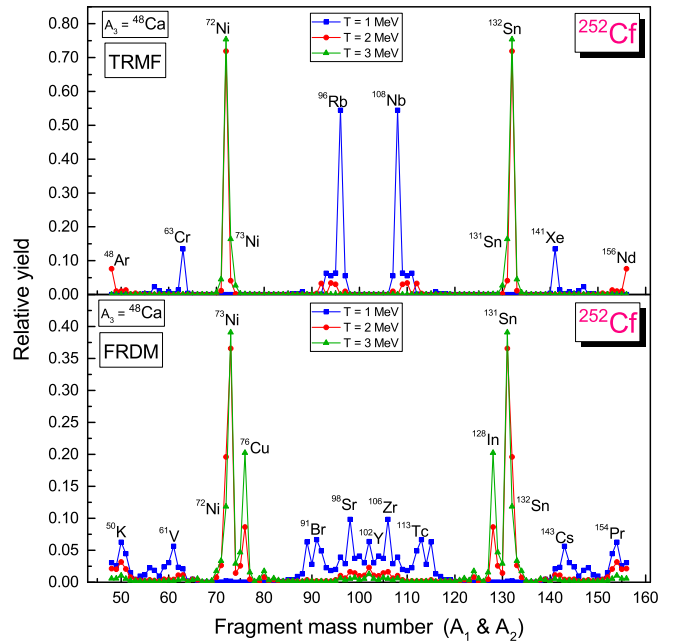


FIG. 4: (Color online) Mass distribution of ^{252}Cf for the fixed third fragment ^{48}Ca for the temperatures $T = 1, 2$ and 3 MeV. The total yield values are normalized to 2.

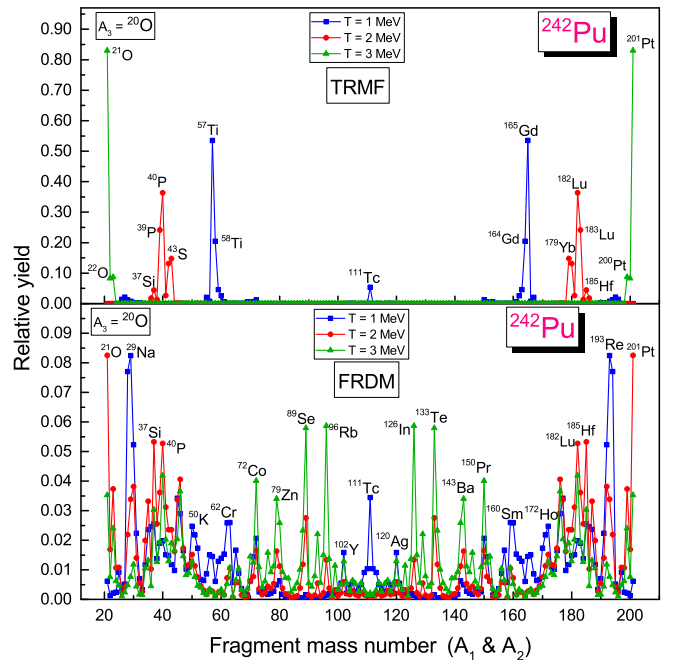


FIG. 5: (Color online) Mass distribution of ^{242}Pu for the fixed third fragment ^{20}O for the temperatures $T = 1, 2$ and 3 MeV. The total yield values are normalized to 2.

for the ternary fission mass distributions of ^{242}Pu and ^{236}U for the fixed third fragments ^{20}O and ^{16}O respectively. At $T = 1$ MeV, we see both symmetric and asymmetric yield for ^{242}Pu and ^{236}U . For the ^{242}Pu , at $T = 1$ MeV, $^{165}\text{Gd} + ^{57}\text{Ti} + ^{20}\text{O}$ is the most favorable combination than the symmetric binary

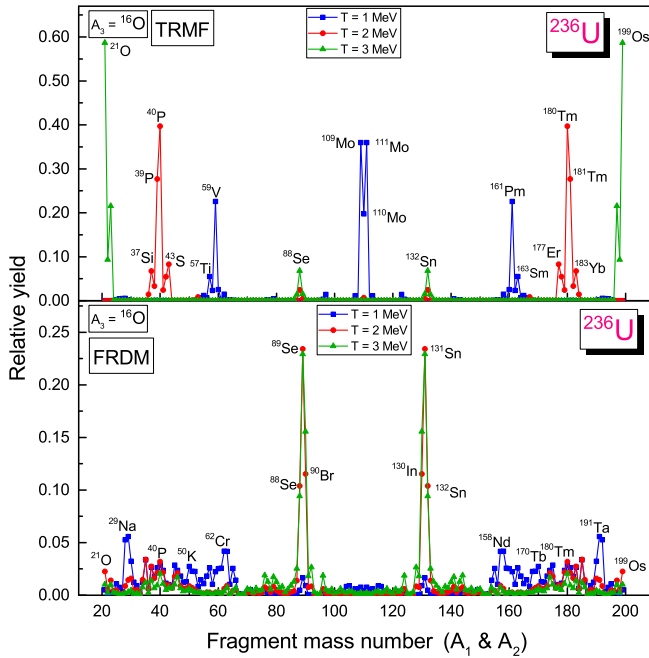


FIG. 6: (Color online) Mass distribution of ^{236}U for the fixed third fragment ^{16}O for the temperatures $T = 1, 2$ and 3 MeV. The total yield values are normalized to 2.

fragments $^{111}\text{Tc} + ^{111}\text{Tc} + ^{20}\text{O}$. For $T = 2$ MeV, $^{182,183}\text{Lu} + ^{40,39}\text{P} + ^{20}\text{O}$, $^{179}\text{Yb} + ^{43}\text{S} + ^{20}\text{O}$ and $^{185}\text{Hf} + ^{37}\text{Si} + ^{20}\text{O}$ are the possible relative yield. At $T = 3$ MeV $^{201}\text{Pt} + ^{21}\text{O} + ^{20}\text{O}$ is the most favorable fragmentation. For ^{236}U , at $T = 1$ MeV, the symmetric breakup into the heavy fragments $^{109}\text{Mo} + ^{111}\text{Mo}$ and $^{110}\text{Mo} + ^{110}\text{Mo}$ along with the third fragment ^{16}O has larger yield values. In addition, the fragment combinations $^{161}\text{Pm} + ^{59}\text{V} + ^{16}\text{O}$ and $^{163}\text{Sm} + ^{57}\text{Ti} + ^{16}\text{O}$ also have larger yield values. For $T = 2$ MeV, $^{180,181}\text{Tm} + ^{40,39}\text{P} + ^{16}\text{O}$ are the most probable fragments. Further, $^{177}\text{Er} + ^{43}\text{S} + ^{16}\text{O}$ and $^{183}\text{Yb} + ^{37}\text{Si} + ^{16}\text{O}$ are also the probable ternary fragments. It is seen that, at $T = 3$ MeV, the fragments $^{199,198,197}\text{Os} + ^{21,22,23}\text{O} + ^{16}\text{O}$ have considerable yield values. In Ref. [16], it is predicted that the ternary charge distribution of ^{252}Cf , at $T = 2$ MeV, with Si, P, S as the most favorable fragments along with Sn and the corresponding partner. Here, at $T = 3$ MeV, the most favorable fragment is one of the closed shell ($Z = 8$) nucleus. Although, one would expect the even-even fragments as more probable for fission, we find large number of odd mass fragments possessing maximum yield compared to even-even. This is due to the fact that the level density of the odd mass fragments are higher than the even mass fragments as reported in Ref. [38].

For the comparison, in Figs. 4 to 6, the FRDM results for the ternary mass distributions are also presented. For the quick reference, the most probable ternary fragmentations and their relative yield values are tabulated in Table I at three different temperatures $T = 1, 2$ and 3 MeV. In general, at $T = 1$ MeV, the most favorable fragments of the FRDM formalism are quite different than those for the TRMF. These differences may be attributed to the differences in the excitation energies

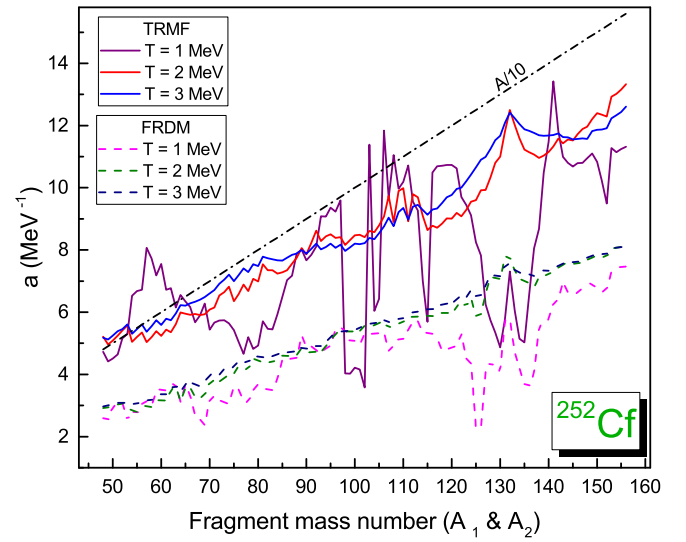


FIG. 7: (Color online) The level density parameter a of the ternary fragmentation of ^{252}Cf for the temperature $T = 1, 2$ and 3 MeV within the TRMF and FRDM formalism.

obtained in the TRMF and FRDM formalisms. For ^{252}Cf the TRMF and FRDM results agree qualitatively with each other at $T = 2$ and 3 MeV. For ^{242}Pu more fragments have considerable yield values in FRDM formalism. At $T = 2$ and 3 MeV, the favorable fragmentations are in the mass range $A_1 \sim 180$ and 130 region with their corresponding partners. The TRMF and FRDM results agree only partially for the ^{242}Pu nucleus at $T = 2$ MeV. For ^{236}U , the most favorable fragments are at $A_1 \sim 130$ for $T = 2$ and 3 MeV in FRDM calculations. One of the favorable fragments has a closed shell nucleon or near closed shell ($N = 82$) nucleus. Further, in both the for-

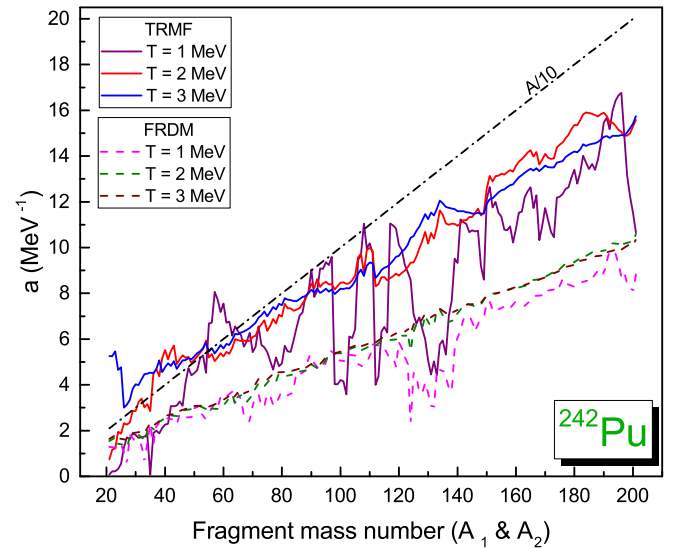


FIG. 8: (Color online) The level density parameter a of the ternary fragmentation of ^{242}Pu for the temperature $T = 1, 2$ and 3 MeV within the TRMF and FRDM formalism.

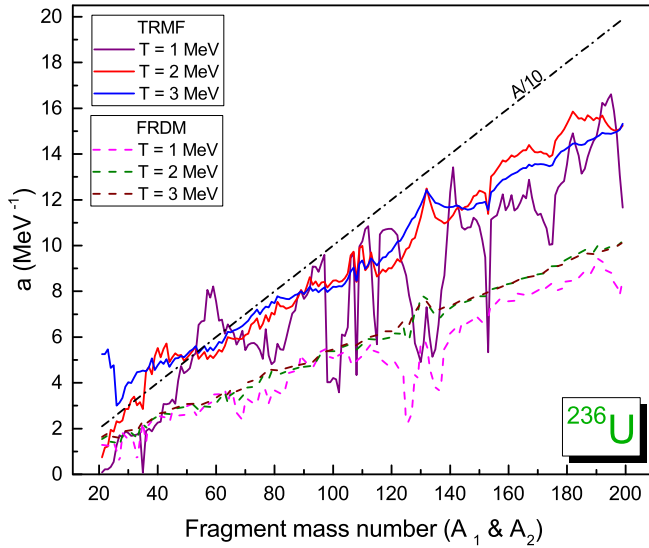


FIG. 9: (Color online) The level density parameter a of the ternary fragmentation of ^{236}U for the temperature $T = 1, 2$ and 3 MeV within the TRMF and FRDM formalism.

malisms, at $T = 2$ MeV, we get nearly similar yield such as ^{40}P along with their partners ^{180}Tm and ^{16}O as shown in Fig. 6. The doubly closed shell nucleus ^{132}Sn is appears in both the cases, at $T = 3$ MeV.

To illustrate the difference between the TRMF and FRDM results, we studied the level density parameter a which is a crucial quantity. In general, the level density parameter a is given by the empirical estimation relation [60]:

$$a = \frac{A}{K} (\text{MeV}^{-1}), \quad (38)$$

where K is the inverse level density parameter, varies from

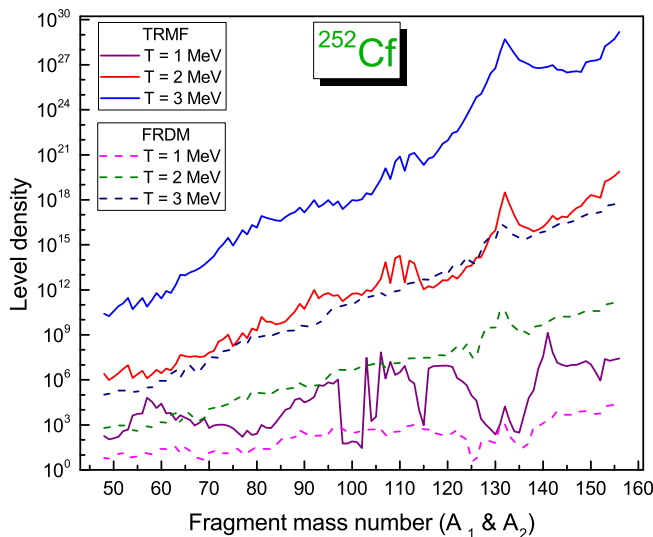


FIG. 10: (Color online) The level density of the ternary fragmentation of ^{252}Cf for the temperature $T = 1, 2$ and 3 MeV.

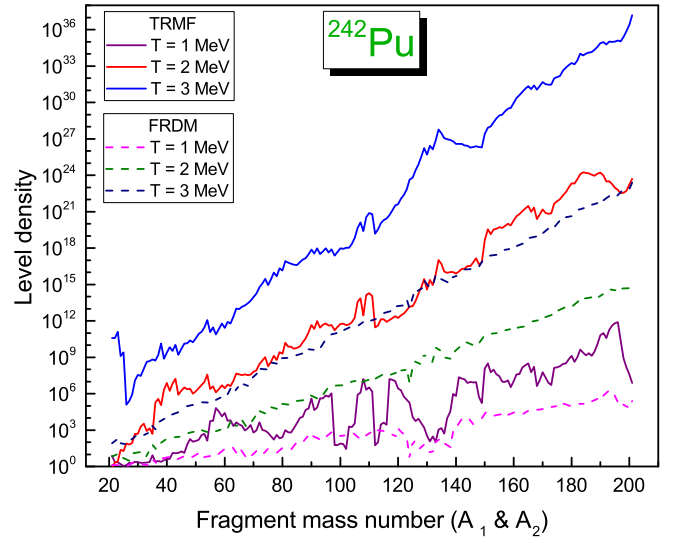


FIG. 11: (Color online) The level density of the ternary fragmentation of ^{242}Pu for the temperature $T = 1, 2$ and 3 MeV.

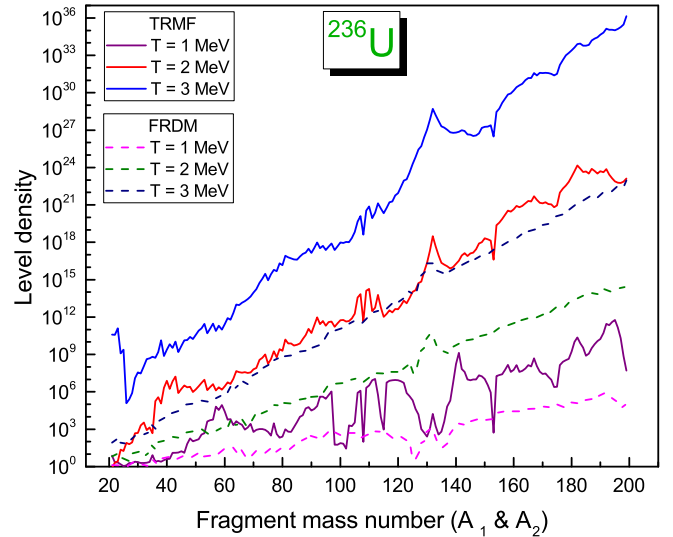


FIG. 12: (Color online) The level density of the ternary fragmentation of ^{236}U for the temperature $T = 1, 2$ and 3 MeV.

10 to 14 depending on the mass number A of the nucleus. In Figs. 7 - 9, we have plotted the level density parameter a of the fission fragments for ^{252}Cf , ^{242}Pu and ^{236}U as a function of mass number. Here, we consider the inverse level density parameter $K = 10$ (which is quite practical value as mentioned in Ref. [60]) for all nuclei and shown in the plots as black dashed dotted line. From these figures, one can see that the TRMF values are very near to the empirical level density parameter a . The FRDM values are considerably lower than the referenced level density parameter. Further, in both models at $T = 1$ MeV, there are more fluctuations in a due to the shell effects of the fission fragments. For ^{252}Cf and ^{236}U , the level density parameter a promptly increases for the doubly closed shell nucleus ^{132}Sn and has the lowest inverse level density

TABLE I: The relative fission yield (R.Y.) = $Y(A_j, Z_j) = \frac{P(A_j, Z_j)}{\sum P(A_j, Z_j)}$ for ^{252}Cf , ^{242}Pu and ^{236}U obtained with TRMF at the temperatures $T = 1, 2$ and 3 MeV are compared with the FRDM prediction (The yield values are normalized to 2).

Parent	T (MeV)	TRMF		FRDM	
		Fragment	R.Y.	Fragment	R.Y.
^{252}Cf	1	$^{108}\text{Nb} + ^{96}\text{Rb} + ^{48}\text{Ca}$	1.090	$^{106}\text{Zr} + ^{98}\text{Sr} + ^{48}\text{Ca}$	0.196
		$^{141}\text{Xe} + ^{63}\text{Cr} + ^{48}\text{Ca}$	0.270	$^{113}\text{Tc} + ^{91}\text{Br} + ^{48}\text{Ca}$	0.134
	2	$^{132}\text{Sn} + ^{72}\text{Ni} + ^{48}\text{Ca}$	1.438	$^{131}\text{Sn} + ^{73}\text{Ni} + ^{48}\text{Ca}$	0.732
		$^{160}\text{Nd} + ^{48}\text{Ar} + ^{48}\text{Ca}$	0.152	$^{132}\text{Sn} + ^{72}\text{Ni} + ^{48}\text{Ca}$	0.392
	3	$^{132}\text{Sn} + ^{72}\text{Ni} + ^{48}\text{Ca}$	1.508	$^{131}\text{Sn} + ^{73}\text{Ni} + ^{48}\text{Ca}$	0.780
		$^{131}\text{Sn} + ^{73}\text{Ni} + ^{48}\text{Ca}$	0.327	$^{128}\text{In} + ^{76}\text{Cu} + ^{48}\text{Ca}$	0.404
^{242}Pu	1	$^{165}\text{Gd} + ^{57}\text{Ti} + ^{20}\text{O}$	1.071	$^{193}\text{Re} + ^{29}\text{Na} + ^{20}\text{O}$	0.165
		$^{164}\text{Gd} + ^{58}\text{Ti} + ^{20}\text{O}$	0.409	$^{111}\text{Tc} + ^{111}\text{Tc} + ^{20}\text{O}$	0.069
		$^{111}\text{Tc} + ^{111}\text{Tc} + ^{20}\text{O}$	0.107	$^{160}\text{Sm} + ^{62}\text{Cr} + ^{20}\text{O}$	0.052
	2	$^{182}\text{Lu} + ^{40}\text{P} + ^{20}\text{O}$	0.726	$^{201}\text{Pt} + ^{21}\text{O} + ^{20}\text{O}$	0.164
		$^{183}\text{Lu} + ^{39}\text{P} + ^{20}\text{O}$	0.482	$^{185}\text{Hf} + ^{37}\text{Si} + ^{20}\text{O}$	0.106
		$^{179}\text{Yb} + ^{43}\text{S} + ^{20}\text{O}$	0.296	$^{182}\text{Lu} + ^{40}\text{P} + ^{20}\text{O}$	0.106
		$^{185}\text{Hf} + ^{37}\text{Si} + ^{20}\text{O}$	0.090	$^{113}\text{Te} + ^{89}\text{Se} + ^{20}\text{O}$	0.056
	3	$^{201}\text{Pt} + ^{21}\text{O} + ^{20}\text{O}$	1.660	$^{126}\text{In} + ^{96}\text{Rb} + ^{20}\text{O}$	0.118
		$^{200}\text{Pt} + ^{22}\text{O} + ^{20}\text{O}$	0.166	$^{133}\text{Te} + ^{89}\text{Se} + ^{20}\text{O}$	0.116
^{236}U	1	$^{111}\text{Mo} + ^{109}\text{Mo} + ^{16}\text{O}$	0.720	$^{191}\text{Ta} + ^{29}\text{Na} + ^{16}\text{O}$	0.112
		$^{161}\text{Pm} + ^{59}\text{V} + ^{16}\text{O}$	0.452	$^{158}\text{Nd} + ^{62}\text{Cr} + ^{16}\text{O}$	0.084
		$^{110}\text{Mo} + ^{110}\text{Mo} + ^{16}\text{O}$	0.395	$^{180}\text{Tm} + ^{40}\text{P} + ^{16}\text{O}$	0.058
	2	$^{180}\text{Tm} + ^{40}\text{P} + ^{16}\text{O}$	0.794	$^{131}\text{Sn} + ^{89}\text{Se} + ^{16}\text{O}$	0.468
		$^{181}\text{Tm} + ^{39}\text{P} + ^{16}\text{O}$	0.554	$^{130}\text{In} + ^{90}\text{Br} + ^{16}\text{O}$	0.230
		$^{177}\text{Er} + ^{43}\text{S} + ^{16}\text{O}$	0.166	$^{180}\text{Tm} + ^{40}\text{P} + ^{16}\text{O}$	0.064
		$^{183}\text{Yb} + ^{37}\text{Si} + ^{16}\text{O}$	0.136	$^{199}\text{Os} + ^{21}\text{O} + ^{16}\text{O}$	0.046
	3	$^{199}\text{Os} + ^{21}\text{O} + ^{16}\text{O}$	1.174	$^{131}\text{Sn} + ^{89}\text{Se} + ^{16}\text{O}$	0.458
		$^{197}\text{Os} + ^{23}\text{O} + ^{16}\text{O}$	0.432	$^{130}\text{Sn} + ^{90}\text{Br} + ^{16}\text{O}$	0.312
		$^{132}\text{Sn} + ^{88}\text{Se} + ^{16}\text{O}$	0.136	$^{132}\text{Sn} + ^{88}\text{Se} + ^{16}\text{O}$	0.188

parameter $K = 10.9$. For ^{242}Pu , the ^{132}Sn nucleus was restricted by Eq. (1). However, value of parameter a increases towards the neutron closed shell ($N = 82$) nuclei. In TRMF model the prompt increase of level density towards the doubly closed shell nucleus ^{132}Sn are clearly seen at $T = 3$ MeV due to the fact all fission fragments becomes spherical Fermi liquid drop as shown in Fig. 3.

To understand the results better we have plotted the level density of the fragments (A_2 and A_1) of the heavy nuclei ^{252}Cf , ^{242}Pu and ^{236}U as a function of mass number as shown in Figs. 10 - 12. From Fig. 10, it can be seen that for $T = 2$ and 3 MeV, the level density of ^{132}Sn is higher than those for the neighboring nuclei in both formalisms. Hence, ^{132}Sn becomes the most favorable fragment. Fig. 12 shows, once again that ^{132}Sn has higher level density than those for the neighboring nuclei, however, the corresponding partner has lower/nearly same level density with the neighboring nuclei in the TRMF model. For the nucleus ^{242}Pu , ^{132}Sn is restricted due to the charge to mass ratio. From Figs. 11 and 12, we see that the fragments Si to S have large level density compared with the neighboring nucleus and the corresponding partners also have the similar behavior. At $T = 3$ MeV, the light charged particles, $Z_2 = 8$ has larger level density than the

neighboring nuclei and its corresponding partners also have the similar behavior. In FRDM formalism, the level density of doubly closed shell nuclei ^{132}Sn has larger value than the neighboring nuclei for ^{252}Cf and ^{236}U at $T = 2$ and 3 MeV. For ^{242}Pu , there is no prompt increase in level density due to the restricted fragment ^{132}Sn by Eq. (1).

Further, from Figs. 10 and 12, it can be seen that the level density promptly increases while reaching the doubly closed shell nucleus ^{132}Sn in both formalisms. It is noted that, other than the light charged particles, ^{132}Sn has the larger level density. This ascertains the fact that with larger the phase space the ternary combinations becomes more probable than the other ternary fragments.

IV. SUMMARY AND CONCLUSIONS

We have studied the mass distribution of ternary fission fragments in ^{252}Cf , ^{242}Pu and ^{236}U nuclei within the statistical theory. Various inputs to the statistical theory, like, the excitation energies and the level density parameters for the different fission fragments at a given temperature are calculated from the TRMF model. The ternary combinations for

these nuclei are obtained from the charge to mass ratio of the parent nuclei. For the comparison, the results obtained using the FRDM inputs to the statistical theory are also presented.

For the nucleus ^{252}Cf we obtained the Sn + Ni + Ca as the most probable ternary combination at the temperatures $T = 2$ and 3 MeV. For the nuclei ^{242}Pu and ^{236}U , however, we obtained few different fragmentations at $T = 2$ and 3 MeV. For these nuclei, at $T = 2$ MeV, the Si/P/S are the possible ternary fragments along with the corresponding fragments. For $T = 3$ MeV, the oxygen isotopes have the larger yield values. The TRMF results for the ^{252}Cf at $T = 2$ and 3 MeV resemble very well with those for the FRDM. Whereas, they strikingly differ from each other at $T = 1$ MeV. In the case of ^{236}U , the mass distributions for the ternary fission fragments corresponding to the TRMF and FRDM resemble each other only at $T = 3$ MeV. For the ^{242}Pu nuclei, the mass distributions for the TRMF model and FRDM are by and large at vari-

ance at all the temperatures considered. Thus, it seems that the mass distribution of the fission fragments are quite sensitive to the effects on the excitation energy and the level density parameter due to the thermal evolution of the deformation and the single-particle energies. This aspects are treated self-consistently within the TRMF model, while, ignored within the later approach.

V. ACKNOWLEDGMENT

The author MTS acknowledge that the financial support from UGC-BSR research grant award letter no. F.25-1/2014-15(BSR)7-307/2010/(BSR) dated 05.11.2015 and IOP, Bhubaneswar for the warm hospitality and for providing the necessary computer facilities.

-
- [1] R. D. Present, Phys. Rev. **59**, 466 (1941).
 [2] Tsien San-Tsiang, Ho Zah-Vei, L. Vignerone, and R. Chastel, Nature **159**, 773 (1947).
 [3] M. L. Muga, C. R. Rice and W. A. Sedlacek, Phys. Rev. **161**, 1266 (1967).
 [4] A. V. Ramayya *et al.*, Phys. Rev. Lett. **81**, 947 (1998); Phys. Rev. C **57**, 2370 (1998).
 [5] U. Köster, H. Faust, G. Fioni, T. Friedrichs, M. Groß and S. Oberstedt, Nucl. Phys. A **652**, 371 (1999).
 [6] Yu. V. Pyatkov *et al.*, Eur. Phys. J. A. **45**, 29 (2010).
 [7] Yu. V. Pyatkov *et al.*, Eur. Phys. J. A. **48**, 94 (2010).
 [8] P. Fong, Phys. Rev. C **3**, 2025 (1971).
 [9] H. Diehl and W. Greiner, Nucl. Phys. A **229**, 29 (1974).
 [10] V. A. Rubchenya and S. G. Yavshits, Z. Phys. A - Atomic Nuclei **329**, 217 (1988).
 [11] W. von Oertzen and A. K. Nasirov, Phys. Lett. B **734**, 234 (2014).
 [12] K. Manimaran and M. Balasubramaniam, Phys. Rev. C **79**, 024610 (2009).
 [13] K. R. Vijayaraghavan, M. Balasubramaniam and W. von Oertzen, Phys. Rev. C **90**, 024601 (2014).
 [14] M. Rajasekaran and V. Devanathan, Phys. Rev. C **24**, 2606 (1981).
 [15] M. Balasubramaniam, C. Karthikraj, N. Arunachalam and S. Selvaraj, Phys. Rev. C **90**, 054611 (2014).
 [16] M. T. Senthil kannan, K. R. Vijayaraghavan, C. Karthikraj, and M. Balasubramaniam, (to be published).
 [17] J. D. Walecka, Ann. Phys., **83**, 491 (1974).
 [18] C. J. Horowitz and B. D. Serot, Nucl. Phys. A **368**, 503 (1981).
 [19] B. D. Serot and J. D. Walecka, Adv. Nucl. Phys. **16**, 1 (1986).
 [20] Y. K. Gambhir, P. Ring and A. Thimet, Ann. of Phys. **198**, 132 (1990).
 [21] S. K. Patra and C. R. Praharaj, Phys. Rev. C **44**, 2552 (1991).
 [22] Y. K. Gambhir, J. P. Maharana, G. A. Lalazissis, P. Panos and P. Ring, Phys. Rev. C **62**, 054610 (2000).
 [23] B. K. Agrawal, Tapas Sil, J. N. De and S. K. Samaddar, Phys. Rev. C **62**, 044307 (2000); *ibid* **63**, 024002 (2001).
 [24] Tapas Sil, B. K. Agrawal, J. N. De, and S. K. Samaddar, Phys. Rev. C **63**, 064302 (2001).
 [25] P. Arumugam, B. K. Sharma, S. K. Patra and R. K. Gupta, Phys. Rev. C **71**, 064308 (2005).
 [26] B. K. Sharma, P. Arumugam, S. K. Patra, P. D. Stevenson, R. K. Gupta and W. Greiner, J. Phys. G. **32**, L1 (2006).
 [27] S. K. Patra, Raj. K. Gupta, B. K. Sharma, P. D. Stevenson and W. Greiner, J. Phys. G. **34**, 2073 (2007).
 [28] W. von Oertzen *et al.*, Eur. Phys. J. A **36**, 279 (2008).
 [29] Raj. K. Gupta, S. K. Patra, P. D. Stevenson, C. Beck, and W. Greiner, J. Phys. G. **35**, 075106 (2008).
 [30] K. Rutz, J. A. Maruhn, P.-G. Reinhard and W. Greiner, Nucl. Phys. A **590**, 680 (1995).
 [31] S. K. Patra, R. K. Choudhury and L. Satpathy, J. Phys. G. **37** 085103 (2010).
 [32] BirBikram Singh, B. B. Sahu and S. K. Patra, Phys. Rev. C **83**, 064601 (2011).
 [33] BirBikram Singh, M. Bhuyan, S. K. Patra and Raj. K. Gupta, J. Phys. G. **39**, 025101 (2012).
 [34] B. B. Sahu, S. K. Singh, M. Bhuyan, S. K. Biswal and S. K. Patra, Phys. Rev. C **89**, 034614 (2014).
 [35] Bharat Kumar, S. K. Singh and S. K. Patra, Int. J. Mod. Phys. **24**, 1550017 (2015).
 [36] Bharat Kumar, S. K. Biswal, S. K. Singh and S. K. Patra, Phys. Rev. C **92**, 054314 (2015).
 [37] G. A. Lalazissis, J. König and P. Ring, Phys. Rev. C **55**, 540 (1997).
 [38] P. Fong, Phys. Rev. **102**, 434 (1956).
 [39] J. R. Huizenga and L. G. Moretto, Annu. Rev. Nucl. Sci. **22**, 427 (1972).
 [40] H. Bethe, Rev. Mod. Phys. **9**, 69 (1937).
 [41] P. Möller, J. R. Nix, W. D. Myers and W. J. Swiatecki, At. Data and Nucl. Data Tables **66**, 131 (1997).
 [42] J. Boguta and A. R. Bodmer, Nucl. Phys. A **292**, 413 (1977).
 [43] C. E. Price and G. E. Walker, Phys. Rev. C **36**, 354 (1987).
 [44] P. G. Blunden and M. J. Iqbal, Phys. Lett. B **196**, 295 (1987).
 [45] P. G. Reinhard, Rep. Prog. Phys. **52**, 439 (1989).
 [46] S. K. Patra, Phys. Rev. C **48**, 1449 (1993).
 [47] M. A. Preston and R. K. Bhaduri, *Structure of Nucleus, Addison-Wesley Publishing Company*, Ch. 8, page 309 (1982).
 [48] D. Vautherin, Phys. Rev. C **7**, 296 (1973).
 [49] J. Dechargé and D. Gogny, Phys. Rev. C **21**, 1568 (1980).
 [50] P. Möller, J. R. Nix and K. L. Kratz, At. Data and Nucl. Data Tables **59**, 185 (1995).
 [51] <https://www-nds.iaea.org/RIPL-3/>

- [52] M. Balasubramaniam and R. K. Gupta, Phys. Rev. C **60**, 064316 (1999).
- [53] J. L. Egidio, L. M. Robledo and V. Martin, Phys. Rev. Lett. **85**, 26 (2000).
- [54] A. L. Goodman, Phys. Rev. C **34**, 1942 (1986).
- [55] NIU Yi-Fei, LINAG Hao-Zhao and MENG Jie, Chin. Phys. Lett. **26**, 032103 (2009).
- [56] B. K. Agrawal, S. K. Samaddar, J. N. De, and S. Shlomo Phys. Rev. C **580**, 3004 (1998).
- [57] W. von Oertzen *et. al.*, Eur. Phys. A **36**, 279 (2008).
- [58] W. von Oertzen *et. al.*, Phys. Rev. C **78**, 044615 (2008).
- [59] K. Manimaran and M. Balasubramaniam, Phys. Rev. C **83**, 034609 (2011).
- [60] B. Nerlo-Pomorska, K. Pomorski, J. Bartel and K. Dietrich, Phys. Rev. C **66**, 051302(R) (2002).